Non-linear elastic in-plane buckling of crown-pinned arches

with rotational end restraints

*K. Luo[1], Y. L. Pi[1], W. Gao[1] and M. A. Bradford[1]

[1] The School of Civil and Environmental Engineering, The University of New South Wales, Sydney, NSW 2052, AUSTRALIA.

*Corresponding author: kai.luo@unsw.edu.au

Abstract

This paper investigates the non-linear elastic in-plane buckling behaviour of a crown-pinned shallow circular arch with rotational end restraints under a uniform radial load or under a central concentrated load. A finite element method and an analytical method are used for the investigation. It is shown that the finite element results agree well with the analytical solutions. It is found that the stiffness of the rotational end restraints has significant effects on the buckling behaviour of arches and that the buckling loads increase with an increase of the stiffness. It is also found that the crown-pin plays an important role in the buckling behaviour of arches. The crown-pinned arches can buckle in a limit point instability mode, but not in a bifurcation mode.

Keywords: Crown-pinned arch, finite element, in-plane buckling, limit point, rotational restraint

Introduction

Studies of the buckling behaviour have been focused on pin-ended and fixed arches (Pi et al. 2002, Bradford et al. 2002). In addition to pin-ended and fixed arches, in engineering structures, an arch is often supported on the elastic foundations or by other structures which provide elastic restraints to the arch ends. Pi et al. (2008) investigated the non-linear in-plane buckling of shallow circular arches with elastic rotational end restraints under a central concentrated load, while Pi and Bradford (2009) reported studies on the non-linear in-plane postbuckling behaviour of shallow circular arches with elastic rotational end restraints under a uniform radial load. In these studies, the arch is assumed to be continuous without any pins between its ends. It is known that in many cases, arches are built by joining two separate curvilinear segments together at the crown, thereby reducing the arch size to meet transport requirements and to create a pin at the arch crown. Because of the crown-pin, the structural responses and buckling behaviour of the arch are different from those of arches without the crown-pin. However, investigations on crown-pinned shallow circular arches with elastic rotational end restraints do not appear to be reported in the open literature.

This paper, therefore, uses both an analytical method and a finite element method to investigate the non-linear in-plane buckling behaviour of crown-pinned shallow circular arches with rotational end restraints subjected to a central point load or to a uniform radial load (Fig. 1).
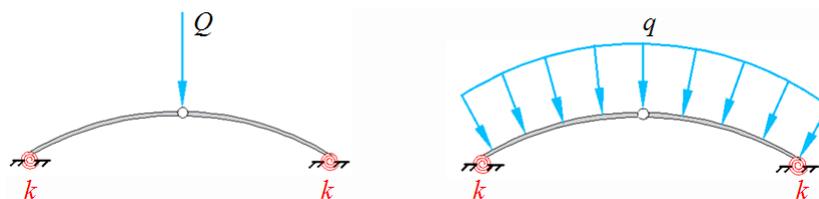
Figure 1. Crown-pinned arches subjected to different loading cases

Non-linear in-plane equilibrium

Assumptions adopted in this investigation are: 1. The Euler-Bernoulli hypothesis is applied. 2. The dimension of the cross-section is much smaller than the length and radius of the arch to ensure sufficient slenderness. Because the arch and load system is symmetric, equilibrium of a half arch ($0 \leq \theta \leq \Theta$ and Θ is half of the included angle of the arch) is considered (Fig. 2). Based on the assumptions, differential equations of equilibrium for a crown-pinned circular arch with equal rotational end restraints can be derived from the principle of virtual work as

$$N' = 0 \quad \text{and} \quad \frac{\tilde{v}^{iv}}{\mu^2} + \tilde{v}'' = -1 \tag{1}$$

for arches that are subjected to a central concentrated load Q (Pi et al. 2008), and as

$$N' = 0 \quad \text{and} \quad \frac{\tilde{v}^{iv}}{\mu^2} + \tilde{v}'' = P \quad \text{with} \quad P = \frac{qR}{N} - 1 \tag{2}$$

for arches that are subjected to a uniform radial load q (Pi and Bradford 2009), where $(\ )' \equiv d(\ )/d\theta$, θ denotes the angular coordinates, $\tilde{v} = v/R$ and $\tilde{w} = w/R$, v and w are the radial and axial displacements with R being the radius of the arch, μ is the dimensionless axial force parameter defined by $\mu = NR^2/EI$ with E being Young's modulus and I being the second moment of area of the cross-section, and the axial compressive force N is defined by

$$N = -AE \int_{-\Theta}^{\Theta} (\tilde{w}' - \tilde{v} + \frac{1}{2}\tilde{v}'^2) \, dA \tag{3}$$
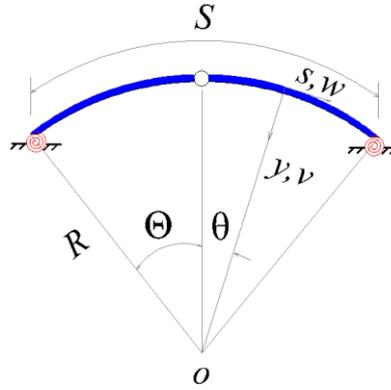
Figure 2. Arch geometry

The static boundary conditions can also be derived as

$$\tilde{v}'' + \frac{\tilde{v}'}{2\Theta\alpha} = 0 \quad \text{at} \quad \theta = \Theta \quad \text{and} \quad \frac{EI}{R}\tilde{v}''' + \frac{\mu^2 EI}{R}\tilde{v}' = \frac{QR}{2} \quad \text{at} \quad \theta = 0 \tag{4}$$

for arches subjected to a central concentrated load Q, and

$$\tilde{v}'' + \frac{\tilde{v}'}{2\Theta\alpha} = 0 \quad \text{at} \quad \theta = \Theta \quad \text{and} \quad \frac{EI}{R}\tilde{v}''' + \frac{\mu^2 EI}{R}\tilde{v}' = 0 \quad \text{at} \quad \theta = 0 \tag{5}$$

for arches subjected to a uniform radial load, where α is the dimensionless restraint flexibility defined by $\alpha = EI/kS$ with k being the stiffness of rotational end restraints and S being the length of the arch.

2

In addition, the kinematic boundary conditions are

$$\tilde{w} = 0 \quad \text{at} \quad \theta = 0 \quad \text{and} \quad \theta = \Theta \quad \text{and} \quad \tilde{v} = 0 \quad \text{at} \quad \theta = \Theta \tag{6}$$

for both loading cases.

Solving the three equations given by Eqs. (1) and (3) or by Eqs. (2) and (3) simultaneously leads to the solution of the radial displacement as

$$
\begin{aligned}
\tilde{v} = & -\frac{1}{2\mu^3 EI\left(2\alpha\beta\sin\beta - \cos\beta\right)}(-2\mu EI\cos\beta\cos\mu\theta + 4\mu\alpha\beta EI\sin\beta\cos\mu\theta - \mu^3\theta^2 EI\cos\beta \\
& + 2\mu^3\theta^2\alpha\beta EI\sin\beta + 2\mu EI - 4\mu\alpha\beta EI\sin\beta - 2\mu\beta EI\sin\beta + \mu\beta^2 EI\cos\beta - 2\mu\alpha\beta^3 EI\sin\beta \\
& + QR^2\sin\beta - QR^2\beta\cos\beta + 2QR^2\alpha\beta^2\sin\beta) + \frac{H(\theta)}{2\mu^3 EI\left(2\alpha\beta\sin\beta - \cos\beta\right)}(2\mu EI\sin\beta\sin\mu\theta \\
& + 4\mu\alpha\beta EI\cos\beta\sin\mu\theta - 4\mu\alpha\beta EI\sin\mu\theta - 2\mu\beta EI\sin\mu\theta + QR^2\sin\mu\theta - QR^2\mu\theta\cos\beta \\
& + 2QR^2\mu\theta\alpha\beta\sin\beta)
\end{aligned}
\tag{7}
$$

for crown-pinned arches subjected to a central concentrated load, and

$$
\begin{aligned}
\tilde{v} = & \frac{P}{2\mu^2\left(\cos\beta - 2\alpha\beta\sin\beta\right)}(2\cos\beta\cos\mu\theta - 4\alpha\beta\sin\beta\cos\mu\theta + \mu^2\theta^2\cos\beta - 2\mu^2\theta^2\alpha\beta\sin\beta \\
& + 2\beta\sin\beta - 2 + 4\alpha\beta\sin\beta - \beta^2\cos\beta + 2\alpha\beta^3\sin\beta) + \frac{H(\theta)P\sin\mu\theta}{\mu^2\left(\cos\beta - 2\alpha\beta\sin\beta\right)}(\sin\beta - \beta \\
& + 2\alpha\beta\cos\beta - 2\alpha\beta)
\end{aligned}
\tag{8}
$$

for crown-pinned arches subjected to a uniform radial load ($\beta = \mu\Theta$), and leads to the non-linear equilibrium equation between the internal force parameter μ and external force Q or q as

$$A_1\tilde{Q}^2 + A_2\tilde{Q} + A_3 = 0 \quad \text{and} \quad B_1 P^2 + B_2 P + B_3 = 0 \tag{9}$$

for the arches subjected to a central concentrated load and to a uniform radial load respectively, where $\tilde{Q}$ is the dimensionless load defined by $\tilde{Q} = R^2\Theta Q/2EI$, and the expressions for coefficients for A_1, A_2, A_3, B_1, B_2 and B_3 are given in Appendix.

The non-linear equilibrium equation between internal force parameter μ and external force Q (or q) given by Eq. (9) has limit points. To determine the limit point, Eq. (9) can be considered as an implicit function of Q (or q) with μ. Hence, the load corresponding to the limit points needs to satisfy

$$\frac{dQ}{d\mu} = -\frac{\partial F(Q,\mu)/\partial\mu}{\partial F(Q,\mu)/\partial Q} = 0 \quad \text{or} \quad \frac{dq}{d\mu} = -\frac{\partial F(q,\mu)/\partial\mu}{\partial F(q,\mu)/\partial q} = 0 \tag{10}$$

Finite element model

The non-linear behaviour of crown-pinned arches is also investigated using the commercial finite

element package ANSYS (2011). The beam element beam188 of ANSYS is herein used to model crown-pinned concrete-filled steel tubular (CFST) arches because the beam188 provides stress stiffness terms, which enable the element to analyse buckling problems. As shown in Figure 3, CFST section is modelled by using two independent subsections which are fully bonded together. To model an arch, 161 nodes connected in sequence lead to 320 elements through the entire arch. It is noted that in ANSYS, the steel tube and the concrete core are generated into separate but fully-bonded elements. To form the pin connection at the crown of the arch, the rotational degree at the crown about z axis is released at which the bending moment vanishes. The combined element combin14 of ANSYS is adopted to model the rotational end restraints at two ends where only rotational movement is allowed so that, to some extent, the bending moment can be transmitted but there are no translational movements. In the element combin14, the stiffness k can be assigned through the relation between load and displacement.
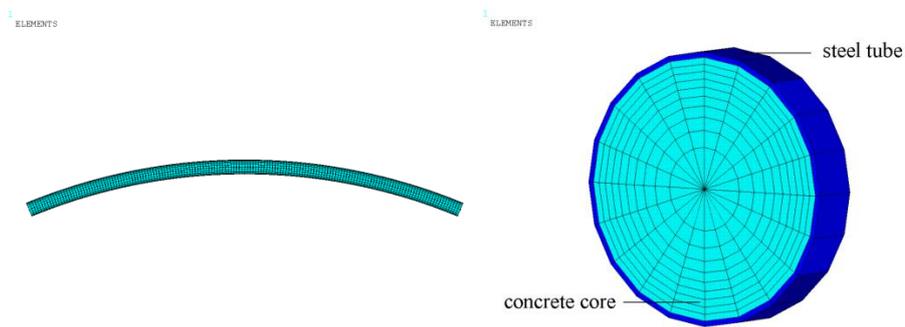
Figure 3. Finite element model of a crown-pinned CFST arch

In non-linear analysis, the switch for the geometric nonlinearity is turned on. The Newton-Raphson method is applied in equilibrium iterations to overcome convergence difficulties. To investigate the buckling behaviour of a crown-pinned arch subjected to different loading cases, the arc-length method is used to ensure numerical stable solutions for the static analysis when external load increases in a step-by-step fashion. Based on the computational results, the buckling behaviour of the crown-pinned arch can be characterized by the load-displacement curve as shown in Figs. 4 and 5, which show the buckling behaviour of a crown-pinned CFST arch under different loading cases along with different boundary conditions: pinned ends, fixed ends and rotationally restrained ends.
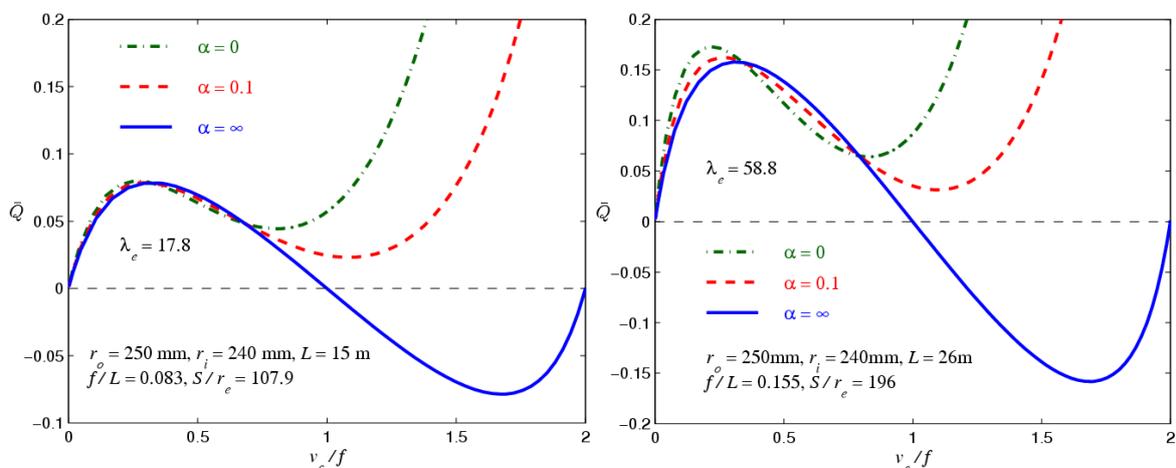
Figure 4. Limit point buckling of rotationally restrained crown-pinned arches under a central concentrated load

4

The geometry of the arch used in the analyses is shown in Figs. 4 and 5 where λ_e is the modified slenderness of the CFST arch defined by $\lambda_e = S\Theta/2r_e$ and r_e is the radius of gyration of the CFST cross-section defined by $r_e = \sqrt{(E_sI_s + E_cI_c)/(A_sE_s + A_cE_c)}$ where E_s and E_c are Young's modulus of the steel tube and core concrete, A_s and A_c are the area of the steel tube and concrete core, and I_s and I_c are the second moment of the area of the steel tube and concrete core, respectively. Also in Figs 4 and 5, $\overline{Q} = Q/N_{cr}$ is the dimensionless central concentrated and N_{cr} is the second mode buckling load of a pinned CFST column about its major axis under uniform axial compression (Pi et al., 2011). When the modified slenderness λ_e is 17.8, the span of the arch is $L = 15$ m with the rise to span ratio $f/L = 0.083$ and the ratio of the arch length to the radius of gyration $S/r_e = 107.9$ which reflects the slenderness of the arch. The stiffness of each rotational end restraint is $k = 1.12\times10^8$ Nm/rad when the dimensionless flexibility of the restraint $\alpha = 0.1$. When $\lambda_e = 58.8$, $L = 26$ m, $f/L = 0.155$ and $S/r_e = 107.9$, the corresponding stiffness is $k = 6.15\times10^7$ Nm/rad if the dimensionless flexibility $\alpha = 0.1$.
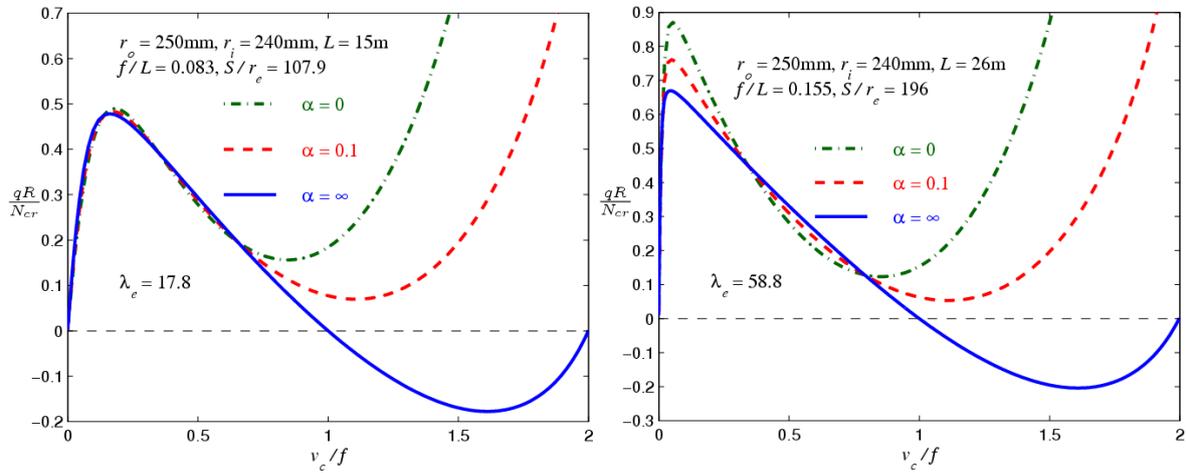
Figure 5. Limit point buckling of rotationally restrained crown-pinned arches under a uniform radial load

It can be seen from Figs. 4 and 5 that when the stiffness vanishes, the arch becomes pin-ended, while when the stiffness approaches infinite, the arch ends are fully fixed. When the stiffness is neither zero nor infinite, the buckling behaviour falls in between these two extreme cases. When λ_e equals 17.8, the limit point buckling load increases slightly with a decrease of the dimensionless flexibility α of rotational end restraints (i.e. with an increase of the corresponding stiffness k). When $\lambda_e = 58.8$, the increase of the buckling load appears to be more substantial. This shows that effects of the stiffness of the rotational end restraints on the buckling behaviour are more significant for deep and slender crown-pinned arches than for their shallow and stocky counterparts. The finite element results show that the crown-pinned arches can buckle in a limit point instability mode, but cannot buckle in a bifurcation mode, which is quite different from arches without the crown-pin that may buckle in a limit point instability mode or in a bifurcation mode.

Comparison of finite element results with analytical solutions

The finite element results are compared with the analytical solutions in Figs. 6 and 7 for the crown-pinned arches with $\lambda_e = 17.8$. It can be seen that the discrepancies between finite element result and their analytical counterparts are extremely small and thus can be neglected. They agree very well with each other. This demonstrates that the finite element model is capable of providing accurate

results for predicting the non-linear in-plane buckling loads of crown-pinned shallow circular arches with rotational end restraints.
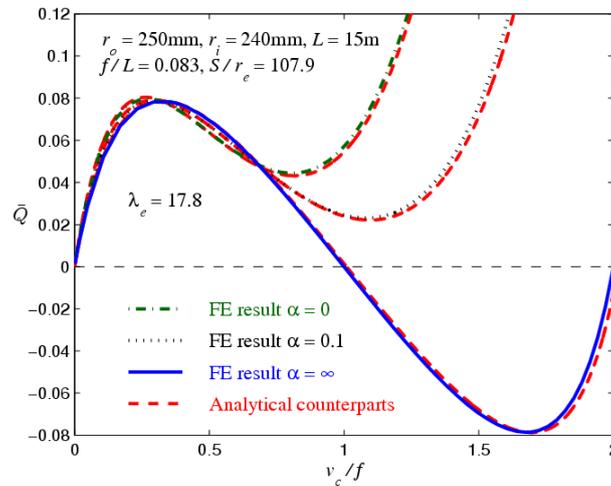
Figure 6. Comparison between analytical and finite element results of limit point buckling of a crown-pinned CFST arch under a central concentrated load
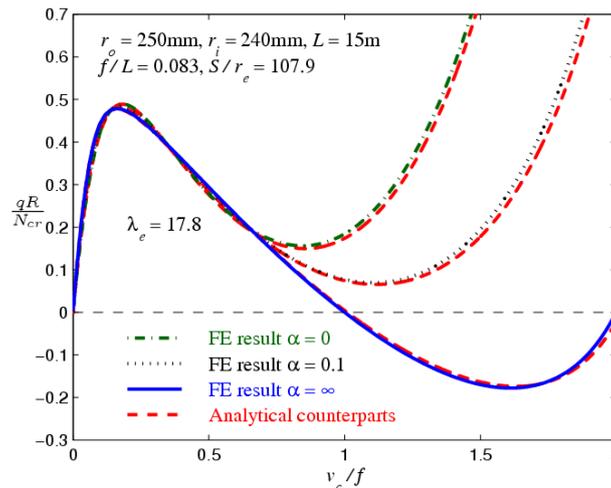
Figure 7. Comparison between analytical and finite element results of limit point buckling of a crown-pinned CFST arch under a uniform radial load

Conclusions

This paper studied the non-linear buckling behaviour of a crown-pinned shallow circular arch with rotational end restraints under a central concentrated load or under a uniform radial load. It was found that the boundary conditions at both ends influence the buckling load of the arch significantly. It was also found that the crown-pin plays an important role in the buckling behaviour of arches. The crown-pinned arches can buckle in a limit point instability mode, but not in a bifurcation mode, which is quite different from arches without the crown-pin that may buckle in a limit point instability mode or in a bifurcation mode. Comparisons of the finite element results with the analytical solutions have shown that the finite element model is capable of providing accurate results for the non-linear buckling behaviour of crown-pinned arches with rotational end restraints.

References

Pi, Y. L., Bradford, M. A. and Uy, B. (2002), In-plane stability of arches. *International Journal of Solids and Structures*, 39(1), pp. 105–125.

Bradford, M. A., Uy, B. and Pi, Y. L. (2002), In-plane stability of arches under a central concentrated load. *Journal of Engineering Mechanics*, 128(7), pp. 710–719.

Pi, Y. L., Bradford, M. A. and Francis, T. L. (2008), Non-linear in-plane buckling of rotationally restrained shallow arches under a central concentrated load. *International Journal of Non-linear Mechanics*, 43, pp. 1–17.

Pi, Y. L., Bradford, M. A. (2009), Non-linear in-plane postbuckling of arches with rotational end restraints under uniform radial loading. *International Journal of Non-Linear Mechanics*, 44(9), pp. 975–989.

Pi, Y. L., Bradford, M. A. and Qu, W. L. (2011), Long-term non-linear behaviour and buckling of shallow concrete-filled steel tubular arches. *International Journal of Non-linear Mechanics*, 46, pp. 1155–1166.

ANSYS, Release 13.0. ANSYS, Inc. Southpointe, 275 Technology Drive, Canonsburg, PA 15317.

Appendix

A_1, A_2 and A_3 for the arch subjected to a central concentrated load are given by

$$A_1 = -\frac{1}{12\psi}(24\alpha^2\beta^3\sin^2\beta - 24\alpha\beta^2\cos\beta\sin\beta - 9\cos\beta\sin\beta + 9\beta$$
$$+ 24\alpha\beta\sin^2\beta - 6\beta\sin^2\beta) \tag{11}$$

$$A_2 = -\frac{1}{24\psi}[-12\beta^3 + 24\alpha\beta^3\cos^2\beta - 72\alpha\beta^3 + (72\alpha\beta^2\sin\beta - 24\beta\cos\beta)(1-\cos\beta)$$
$$+ (12\beta^2\sin\beta + 24\alpha\beta^3\cos\beta)(1+\cos\beta)] \tag{12}$$

$$A_3 = \frac{\beta^2}{\lambda^2} - \frac{1}{48\psi}[(48\alpha\beta^5 + 96\alpha^2\beta^5 - 96\alpha^2\beta^4\sin\beta - 12\beta^4\sin\beta - 96\alpha\beta^4\sin\beta)(1-\cos\beta)$$
$$- 12\beta^2\sin\beta\cos\beta + 12\beta^3 - 12\beta^4\sin\beta + 4\beta^5 + 8\beta^5\sin^2\beta + 48\alpha\beta^3\sin^2\beta$$
$$- 48\alpha\beta^4\sin\beta\cos\beta + 32\alpha\beta^6\sin\beta\cos\beta - 32\alpha^2\beta^7\sin^2\beta] \tag{13}$$

with ψ and λ defined by

$$\psi = \beta^5(-\cos^2\beta + 4\alpha\beta\sin\beta\cos\beta - 4\alpha^2\beta^2\sin^2\beta) \tag{14}$$

$$\lambda = \frac{S\Theta}{2r_e} \tag{15}$$

and B_1, B_2 and B_3 for for crown-pinned arches subjected to a uniform radial load are given by

$$B_1 = \frac{1}{12\zeta}(-24\beta\cos\beta - 36\alpha\beta^3 - 3\beta - 36\alpha\beta + 6\beta^2\sin\beta + 15\cos\beta\sin\beta - 48\alpha\beta\cos\beta$$
$$+ 84\alpha\beta\cos^2\beta - 3\beta^3 - 8\alpha^2\beta^5 + 72\alpha\beta^2\sin\beta + 24\alpha^2\beta^3\cos\beta + 120\alpha^2\beta^2\sin\beta$$
$$+ 12\alpha\beta^3\cos\beta - 12\alpha\beta^2\cos\beta\sin\beta + 48\alpha^2\beta^3\cos^2\beta - 120\alpha^2\beta^2\cos\beta\sin\beta - 72\alpha^2\beta^3$$
$$+ 9\beta^2\sin\beta\cos\beta + 8\alpha\beta^4\cos\beta\sin\beta + 24\alpha\beta^3\cos^2\beta + 8\alpha^2\beta^5\cos^2\beta + 12\beta\cos^2\beta$$
$$- 2\beta^3\cos^2\beta) \tag{16}$$

7

$$B_2 = \frac{1}{12\zeta}(-16\alpha^2\beta^5 + 12\cos\beta\sin\beta + 48\alpha\beta^2\sin\beta + 72\alpha\beta\cos^2\beta - 24\alpha\beta - 24\alpha\beta^3$$
$$- 48\alpha\beta\cos\beta - 24\beta\cos\beta - 48\alpha^2\beta^3 + 96\alpha^2\beta^2\sin\beta + 16\alpha\beta^4\cos\beta\sin\beta - 4\beta^3\cos^2\beta \qquad (17)$$
$$+ 12\beta\cos^2\beta + 12\beta^2\cos\beta\sin\beta + 48\alpha^2\beta^3\cos^2\beta - 96\alpha^2\beta^2\cos\beta\sin\beta + 16\alpha^2\beta^5\cos^2\beta$$
$$+ 24\alpha\beta^3\cos^2\beta)$$

$$B_3 = \frac{\beta^2}{\lambda^2} \qquad (18)$$

with ζ defined by

$$\zeta = \beta^3(-\cos^2\beta + 4\alpha\beta\cos\beta\sin\beta - 4\alpha^2\beta^2\sin^2\beta) \qquad (19)$$